Mathematics

AIMS Mathematics, 10(12): 28129–28150.
DOI: 10.3934/math.20251237
Received: 15 September 2025
Revised: 14 November 2025
Accepted: 21 November 2025
Published: 01 December 2025

https://www.aimspress.com/journal/Math

Research article

Nonlinear vibration reduction in vertical conveyor systems using a nonlinear integral negative derivative feedback controller

R. E. Abdullah[1,*], Rageh K. Hussein[2], Y. A. Amer[3], O. M. Khaled[4], Mohamed Ibrahim Attia[5], Asmaa M. Abd-Elal[4] and M. N. Abd El-Salam[6]

[1] Department of Mathematics, Saxony Egypt University for Applied Science and Technology, Cairo 11511, Egypt
[2] Physics Department, College of Science, Imam Mohammad Ibn Saud Islamic University (IMSIU), Riyadh 11623, Saudi Arabia
[3] Mathematics Department, Science Faculty, Zagazig University, Zagazig, Egypt
[4] Department of Mathematical and Computer Science, Faculty of Sci. Port Said University, Port Said, Egypt
[5] Chemistry Department, College of Science, Imam Mohammad Ibn Saud Islamic University (IMSIU), Riyadh 11623, Saudi Arabia
[6] Department of Basic Sciences, Common First Year Deanship, King Saud University, Riyadh 12373, Saudi Arabia

* **Correspondence:** Email: redaabdallah316@gmail.com.

Abstract: This paper presents an advanced control strategy to suppress nonlinear vibrations in a vertical conveyor system subjected to simultaneous resonance. Vertical conveyors play a crucial role in industrial applications, where stability and continuous performance are essential. However, excessive vibrations can reduce efficiency, cause mechanical fatigue, and increase maintenance costs. To describe the dynamics, the system is modeled as a multi-degree-of-freedom cantilever beam with quadratic and cubic nonlinearities under external harmonic excitations. These nonlinearities introduce complex behaviors, especially when internal and external resonances interact. Previous studies have analyzed the system using the multiple scale perturbation technique (MSPT) to investigate dynamic responses and resonance conditions. While this approach provides valuable insights, controlling nonlinear vibrations requires more effective strategies than conventional controllers. In this work, we propose a nonlinear integral negative derivative feedback (NINDF) controller, which combines first-order and second-order filters. This structure enhances stability

margins, improves robustness, and ensures better vibration suppression during critical resonance states. Analytical solutions were derived via MSPT, and system stability was assessed using the Routh-Hurwitz criterion. Additionally, the system equations were integrated using the classical fourth-order Runge-Kutta (RK4) method, which provides reliable accuracy for short-term transient simulations. However, RK4 does not inherently preserve the geometric invariants (e.g., energy and phase-space structure) that are significant in nonlinear systems exhibiting internal resonance. Results demonstrate that the NINDF controller effectively reduces vibration amplitudes, particularly under 1:1 internal resonance, and achieves superior performance compared to traditional feedback methods. Hence, the proposed control strategy offers a practical and reliable tool for mitigating nonlinear vibrations in engineering systems exposed to demanding dynamic environments.

Keywords: vertical conveyor; NINDF; MSPT; simultaneous resonance; nonlinear vibration; stability analysis; negative feedback control
Mathematics Subject Classification: 34C15, 34C46, 34F15, 74G10, 70H03

1. Introduction

In recent years, the study of nonlinear vibrations in engineering structures has received increasing attention due to their significant impact on dynamic performance and structural stability. Vertical conveyor systems and cantilever-type configurations are widely used in mechanical, aerospace, and civil engineering because they can carry loads without intermediate supports. However, these systems often exhibit complex vibration phenomena, particularly under harmonic and parametric excitations [1–3]. To analyze such behaviors, multi-scale perturbation methods have been extensively employed to investigate primary, subharmonic, and superharmonic responses, while mathematical software has facilitated the evaluation of motion parameters and stability conditions [4]. Nonlinear dynamic models incorporating quadratic and cubic nonlinearities are commonly adopted for vertical conveyor systems, often treated as multi-degree-of-freedom (MDOF) structures. Bauomy and El-Sayed [5] studied a 2-DOF nonlinear vertical conveyor subjected to dual-frequency excitation using the multiple-scales perturbation technique (MSPT), revealing strong interactions between internal and external resonances. Their work was later extended to a 4-DOF configuration [6], where positive position feedback (PPF) controllers were implemented for vibration suppression. Although PPF was effective for primary resonance, it lacked robustness under simultaneous resonance conditions. Amer et al. [7] further examined dual-resonance behaviors and proposed saturation-based absorbers, which reduced large-amplitude responses but only within limited parameter ranges. Nonlinear oscillators excited by harmonic or parametric forces, such as Rayleigh- and Duffing-type systems, have also been investigated for bifurcation and stability characteristics [8–10]. The coexistence of internal and external resonances has motivated the development of more advanced control strategies. Asymptotic solutions for cantilever beams with lumped masses have been derived using the homotopy analysis method (HAM) and the differential transformation method (DTM) [11,12]. Meanwhile, traditional approaches such as negative derivative feedback (NDF) [13], integral resonant control (IRC) [14], and saturation-based absorbers [7] suffer from limited adaptability and robustness. For instance, Shen et al. [15] demonstrated that self-excited oscillations in unforced systems require more sophisticated suppression mechanisms than linear damping, while

other studies [16,17] showed that time-delayed PPF controllers for Rayleigh-Van der Pol-Duffing oscillators are highly sensitive to delay and loop gain. To address these challenges, a hybrid control strategy—the nonlinear integral-negative derivative feedback (NINDF) controller—has been introduced. The method integrates a first-order filter for damping regulation with a second-order filter for energy redistribution at resonance, providing an adaptive solution for nonlinear vibration control [18,19]. This research investigates various approaches to vibration control and performance enhancement in engineering systems. The first study analyzes the impact of proportional derivative control on reducing vibrations and improving the performance of permanent magnet synchronous motors. The second study applies a negative derivative feedback controller to mitigate vibrations in a hybrid Rayleigh-Van der Pol-Duffing oscillator, enhancing system stability in nonlinear environments. The third paper examines model predictive torque control for a multilevel power converter in four-phase switched reluctance motors, aiming to optimize dynamic performance and efficiency. Finally, the fourth study explores the size-dependent vibrations in laminated functionally graded curved beams with piezoelectric layers, providing insights into vibration behavior and contributing to the design optimization of such materials [20–24].

In this study, a novel NINDF controller is developed and implemented for a 2-DOF nonlinear vertical conveyor system exhibiting 1:1 internal resonance. The controller aims to suppress complex vibratory interactions and enhance system stability under simultaneous resonance conditions. The governing nonlinear equations are formulated, and analytical solutions are derived via the multiple scales perturbation technique (MSPT). The frequency response equations (FREs) and stability domains are determined using the Routh–Hurwitz criterion, while numerical simulations based on the fourth-order Runge-Kutta method confirm the analytical outcomes. Comparative evaluations against established controllers demonstrate the superior damping efficiency and robustness of the proposed NINDF strategy. Unlike conventional schemes, the NINDF controller achieves rapid attenuation of oscillations and sustained stability even under strong nonlinear coupling. By integrating the resonance-compensation capability of IRC with the inherent damping strength of NDF, it provides a more adaptive and resilient control framework. These findings establish NINDF as a highly effective approach for advanced nonlinear vibration suppression in multi-resonant mechanical systems.

This paper is organized as follows: The Abstract summarizes the study's aim, methods, and key findings on vibration suppression using the NINDF controller. Section 1 (Introduction) reviews nonlinear vibration challenges and motivates the proposed control approach. Section 2 (Formulation of the problem) presents the nonlinear multi-degree-of-freedom model and control equations. Section 3 (Mathematical analysis) applies the multiple scales perturbation technique to derive analytical solutions and resonance conditions. Section 4 (Stability analysis) uses the Routh-Hurwitz criterion and eigenvalue analysis to assess system stability. Section 5 (Results and discussion) provides numerical simulations based on RK4, illustrating the system's behavior before and after control. Section 6 (Comparative study) compares NINDF performance with PD, PPF, and NSC controllers, while Section 7 (Numerical accuracy discussion) evaluates RK4 against symplectic methods. Finally, Section 8 (Conclusion) highlights the controller's effectiveness and suggests structure-preserving schemes for future work, with detailed derivations and supplementary data included in the appendices. All used parameters in Eqs (1)–(6) listed in Table 1.

Table 1. Used symbols.

$z,\dot{z},\ddot{z}$	$\psi,\dot{\psi},\ddot{\psi}$	Displacements, velocities, and accelerations of the mean system.
$u,\dot{u},\ddot{u}$	$v,\dot{v},\ddot{v}$	Displacements, velocities, and accelerations of the controller.
$\dot{p},p$	$\dot{q},q$	Dimensionless motion and velocities of the controller.
f_1	f_2	Amplitude of external forces.
ω_1,ω_2	ω_3,ω_4	Natural frequencies of the main system and controller, respectively.
β_1,β_2	β_3,β_4	Nonlinear stiffness coefficients (quadratic and cubic).
Ω_1,Ω_2	Ω_3,Ω_4	Excitation frequencies.
$\gamma_1,\gamma_2,\gamma_3,\gamma_4$	$\lambda_1,\lambda_2,\lambda_3,\lambda_4$	Dimensionless control and feedback signal gains, respectively.
μ_1	μ_2	Damping coefficients for $\dot{z},\dot{\psi}$.
α_1	α_2	Damping coefficients for $\dot{u},\dot{v}$.
δ_1	δ_2	Lossy integrator's frequency coefficient for p,q.
ε	ε	Small perturbation parameter $(\varepsilon >> 1)$.

2. Formulation of the problem

Figure 1(a) depicts the vibrating model of a vertical shaking conveyor, as provided in [3], where the model is subjected to many harmonic excitations. We create the block diagram for the simulation of this model, as shown below.

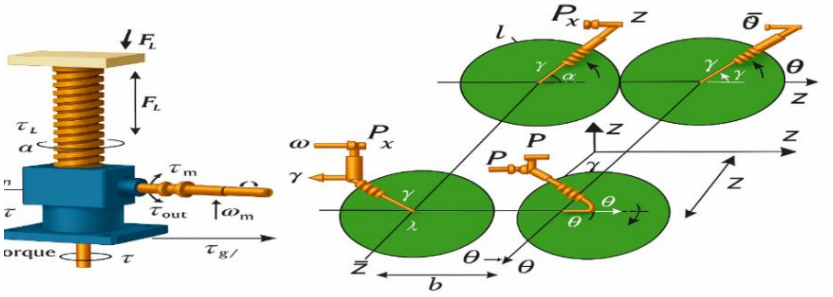

(a)

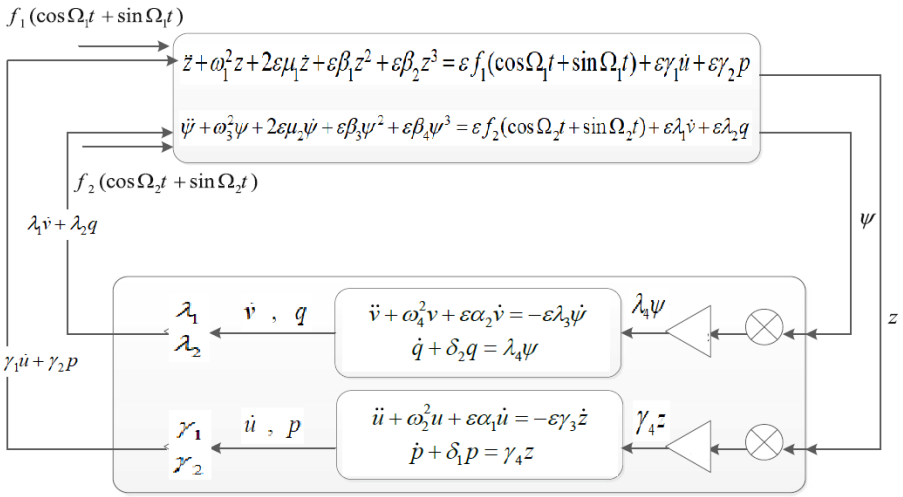

(b)

Figure 1. (a) Vertical shaking conveyor schematic diagram; (b) Closed-loop control system of the vertical shaking conveyor.

The equations of motion governing the model in non-dimensional form [3] were adjusted as follows:

$$\ddot{z} + \omega_1^2 z + 2\varepsilon\mu_1\dot{z} + \varepsilon\beta_1 z^2 + \varepsilon\beta_2 z^3 = \varepsilon f_1(\cos\Omega_1 t + \sin\Omega_1 t) + \varepsilon\gamma_1\dot{u} + \varepsilon\gamma_2 p, \tag{1}$$

$$\ddot{\psi} + \omega_3^2\psi + 2\varepsilon\mu_2\dot{\psi} + \varepsilon\beta_3\psi^2 + \varepsilon\beta_4\psi^3 = \varepsilon f_2(\cos\Omega_2 t + \sin\Omega_2 t) + \varepsilon\lambda_1\dot{v} + \varepsilon\lambda_2 q. \tag{2}$$

We will use the NINDF controller. It combines two types of controls: IRC control and NDF control. These work together to suppress the vibrations of the investigated system as follows:

$$\ddot{u} + \omega_2^2 u + \varepsilon\alpha_1\dot{u} = -\varepsilon\gamma_3\dot{z}, \tag{3}$$

$$\ddot{v} + \omega_4^2 v + \varepsilon\alpha_2\dot{v} = -\varepsilon\lambda_3\dot{\psi}, \tag{4}$$

$$\dot{p} + \delta_1 p = \gamma_4 z, \tag{5}$$

$$\dot{q} + \delta_2 q = \lambda_4\psi. \tag{6}$$

3. Mathematical analysis

For Eqs (1)–(6), an approximate analytical solution is obtained independently using the multiple scales method [25,26]. We are looking for a first-order expansion in the form

$$\left.\begin{aligned} z(t,\varepsilon) &= z_0(T_0,T_1) + \varepsilon z_1(T_0,T_1) + o(\varepsilon^2) \\ \psi(t,\varepsilon) &= \psi_0(T_0,T_1) + \varepsilon\psi_1(T_0,T_1) + o(\varepsilon^2) \\ u(t,\varepsilon) &= u_0(T_0,T_1) + \varepsilon u_1(T_0,T_1) + o(\varepsilon^2) \\ v(t,\varepsilon) &= v_0(T_0,T_1) + \varepsilon v_1(T_0,T_1) + o(\varepsilon^2) \\ p(t,\varepsilon) &= p_0(T_0,T_1) + \varepsilon p_1(T_0,T_1) + o(\varepsilon^2) \\ q(t,\varepsilon) &= q_0(T_0,T_1) + \varepsilon q_1(T_0,T_1) + o(\varepsilon^2) \end{aligned}\right\}. \tag{7}$$

Derivatives can be written as follows:

$$\frac{d}{dt} = D_0 + \varepsilon D_1 + \ldots \tag{8}$$

$$\frac{d^2}{dt^2} = D_0^2 + 2\varepsilon D_0 D_1 + \ldots \tag{9}$$

Let us introduce the derivatives and the two time scales for the first-order approximation, where $T_n = \varepsilon^n t$ and $D_n = \frac{\partial}{\partial T_n}$, $(n = 0,1)$. Substituting Eqs (7)–(9) into Eqs (1)–(6) and equating coefficients of like powers ε , we obtain:

$$o(\varepsilon^0): \quad \left.\begin{aligned} &(D_0^2+\omega_1^2)z_0 = 0\\ &(D_0^2+\omega_3^2)\psi_0 = 0\\ &(D_0^2+\omega_2^2)u_0 = 0\\ &(D_0^2+\omega_4^2)v_0 = 0\\ &(D_0+\delta_1)p_0 = \gamma_4 z_0\\ &(D_0+\delta_2)q_0 = \lambda_4\psi_0 \end{aligned}\right\}, \tag{10}$$

$$o(\varepsilon^1): \quad \left.\begin{aligned} &(D_0^2+\omega_1^2)z_1 = -2D_1D_0z_0 - 2\mu_1D_0z_0 - \beta_1z_0^2 - \beta_2z_0^3 + \varepsilon f_1(\cos\Omega_1 t + \sin\Omega_1 t) + \gamma_1D_0u_0 + \gamma_2p_0\\ &(D_0^2+\omega_3^2)\psi_1 = -2D_1D_0\psi_0 - 2\mu_2D_0\psi_0 - \beta_3\psi_0^2 - \beta_4\psi_0^3 + \varepsilon f_2(\cos\Omega_2 t + \sin\Omega_2 t) + \lambda_1D_0v_0 + \lambda_2q_0\\ &(D_0^2+\omega_2^2)u_1 = -2D_1D_0u_0 - \alpha_1D_0u_0 - \gamma_3D_0z_0\\ &(D_0^2+\omega_4^2)v_1 = -2D_1D_0v_0 - \alpha_2D_0v_0 - \lambda_3D_0\psi_0\\ &(D_0+\delta_1)p_1 = \gamma_4z_1 - D_1p_0\\ &(D_0+\delta_2)q_1 = \lambda_4\psi_1 - D_1q_0 \end{aligned}\right\}. \tag{11}$$

We write the solutions to Eq (10) in the form:

$$\left.\begin{aligned} &z_0(T_0,T_1) = Ae^{i\omega_1T_0} + \bar{A}e^{-i\omega_1T_0}\\ &\psi_0(T_0,T_1) = Ee^{i\omega_2T_0} + \bar{E}e^{-i\omega_2T_0}\\ &u_0(T_0,T_1) = Ce^{i\omega_3T_0} + \bar{C}e^{-i\omega_3T_0}\\ &v_0(T_0,T_1) = Ye^{i\omega_4T_0} + \bar{Y}e^{-i\omega_4T_0}\\ &p_0(T_0,T_1) = \frac{\delta_1 - i\omega_1}{\delta_1^2+\omega_1^2}\gamma_4Ae^{i\omega_1T_0} + Q_1e^{-\delta_1T_0} + c.c.\\ &q_0(T_0,T_1) = \frac{\delta_2 - i\omega_3}{\delta_2^2+\omega_3^2}\lambda_4Ee^{i\omega_3T_0} + Q_2e^{-\delta_2T_0} + c.c. \end{aligned}\right\}, \tag{12}$$

where A,E,C,Y are complex functions in T_1, and Q_1, Q_2 are constants of integration resulting from the values of each p_0, q_0. By substituting Eq (12) into Eq (11), we obtain the following:

$$\left.\begin{aligned} &(D_0^2+\omega_1^2)z_1 = (-2iD_1\omega_1A - 2i\mu_1\omega_1A - 3\beta_2A^2\bar{A} + +\gamma_2\gamma_4\frac{\delta_1 - i\omega_1}{\delta_1^2+\omega_1^2}A)e^{i\omega_1T_0}\\ &-\beta_1(A^2e^{2i\omega_1T_0} + 2A\bar{A}) - \beta_2A^3e^{3i\omega_1T_0} + i\omega_2\gamma_1ce^{i\omega_2T_0} + \frac{f_1}{2}(e^{i\Omega_1T_0} - ie^{i\Omega_1T_0}) + c.c.\\ &(D_0^2+\omega_3^2)\psi_1 = (-2iD_1\omega_3E - 2i\mu_2\omega_3E - 3\beta_4E^2\bar{E} + \lambda_2\lambda_4\frac{\delta_2 - i\omega_3}{\delta_2^2+\omega_3^2}E)e^{i\omega_3T_0}\\ &-\beta_3(E^2e^{2i\omega_3T_0} + 2E\bar{E}) - \beta_4E^3e^{3i\omega_3T_0} + i\omega_4\lambda_1Ye^{i\omega_4T_0} + \frac{f_2}{2}(e^{i\Omega_2T_0} - ie^{i\Omega_2T_0}) + c.c.\\ &(D_0^2+\omega_2^2)u_1 = (-2i\omega_2D_1c - i\omega_2\alpha_1c)e^{i\omega_2T_0} - i\omega_1\gamma_3Ae^{i\omega_1T_0} + c.c.\\ &(D_0^2+\omega_4^2)v_1 = (-2i\omega_4D_1Y - i\omega_4\alpha_2Y)e^{i\omega_4T_0} - i\omega_3\lambda_3Ee^{i\omega_3T_0} + c.c. \end{aligned}\right\}. \tag{13}$$

After eliminating all secular terms in Eq (13), $z_1, \psi_1, u_1, v_1, p_1$, and q_1 take the following forms:

$$\left.\begin{aligned}
&z_1(T_0,T_1) = N_1(T_1)e^{2i\omega_1 T_0} + N_2(T_1) + N_3(T_1)e^{3i\omega_1 T_0} + N_4(T_1)e^{i\omega_2 T_0} + N_5(T_1)(e^{i\Omega_1 T_0} - ie^{i\Omega_1 T_0}) + c.c.\\
&\psi_1(T_0,T_1) = L_1(T_1)e^{2i\omega_3 T_0} + L_2(T_1) + L_3(T_1)e^{3i\omega_3 T_0} + L_4(T_1)e^{i\omega_4 T_0} + L_5(T_1)(e^{i\Omega_2 T_0} - ie^{i\Omega_2 T_0}) + c.c.\\
&u_1(T_0,T_1) = N_6(T_1)e^{i\omega_1 T_0} + c.c.\\
&v_1(T_0,T_1) = L_6(T_1)e^{i\omega_3 T_0} + c.c.\\
&p_1(T_0,T_1) = N_7(T_1)e^{2i\omega_1 T_0} + N_8(T_1)e^{3i\omega_1 T_0} + N_9(T_1) + N_{10}(T_1)e^{i\omega_2 T_0} +\\
&\qquad N_{11}(T_1)(e^{i\Omega_1 T_0} - ie^{i\Omega_1 T_0})) + N_{12}(T_1)e^{i\omega_1 T_0} + N_{13}(T_1)e^{-\delta_1 T_0} + g(T_1) + c.c.\\
&q_1(T_0,T_1) = L_7(T_1)e^{2i\omega_3 T_0} + L_8(T_1)e^{3i\omega_3 T_0} + L_9(T_1) + L_{10}(T_1)e^{i\omega_4 T_0}\\
&\qquad + L_{11}(T_1)(e^{i\Omega_2 T_0} - ie^{i\Omega_2 T_0})) + L_{12}(T_1)e^{i\omega_3 T_0} + L_{13}(T_1)e^{-\delta_2 T_0} + m(T_1) + c.c.
\end{aligned}\right\} \tag{14}$$

where L_i, N_i and $i = 1,2,...,13$ appear in Appendix A. The complex conjugate components are gathered under the symbol c.c. From Eq (13), we can list all resonance cases, which might be stated as:

a. Primary resonance case $\Omega_i = \omega_i, i = 1,2$;

b. Internal resonance case $\omega_j = \omega_i, j = 3,4$;

c. Simultaneous resonance case: any combination of the two previous cases.

4. Periodic solutions

Simultaneous resonance is the worst type of resonance: $\Omega_1 = \omega_1, \Omega_2 = \omega_2$ and $\omega_1 = \omega_3, \omega_2 = \omega_4$. In order to discuss the conditions of the solution, the tuning parameters of equations σ_1 and σ_2 are identified as follows:

$$\Omega_1 = \omega_1 + \varepsilon\sigma_1, \omega_2 = \omega_1 + \varepsilon\sigma_2. \tag{15}$$

When Eq (15) is added to Eq (13), the solvability conditions take the following forms:

$$\left.\begin{aligned}
&-2i\omega_1 D_1 A - 2i\mu_1\omega_1 A - 3\beta_2 A^2\bar{A} + \gamma_2\gamma_4\frac{\delta_1 - i\omega_1}{\delta_1^2 + \omega_1^2}A + i\omega_2\gamma_1 C e^{i\sigma_2 T_1} + \frac{f_1}{2}(e^{i\sigma_1 T_1} - ie^{i\sigma_1 T_1}) = 0\\
&-2i\omega_3 D_1 E - 2i\mu_2\omega_3 E - 3\beta_4 E^2\bar{E} + \lambda_2\lambda_4\frac{\delta_2 - i\omega_3}{\delta_2^2 + \omega_3^2}E + i\omega_4\lambda_1 Y e^{i\sigma_4 T_1} + \frac{f_2}{2}(e^{i\sigma_3 T_1} - ie^{i\sigma_3 T_1}) = 0\\
&-2i\omega_2 D_1 C - i\omega_2\alpha_1 C - i\omega_1\gamma_3 A e^{-i\sigma_2 T_1} = 0\\
&-2i\omega_4 D_1 Y - i\omega_4\alpha_3 Y - i\omega_3\lambda_3 E e^{-i\sigma_4 T_1} = 0
\end{aligned}\right\}. \tag{16}$$

Putting A, C, H, and Y in the polar form, it appears as follows:

$$\left.\begin{aligned}
&A(T_1)=\frac{1}{2}a(T_1)e^{i\theta_1(T_1)},\ C(T_1)=\frac{1}{2}c(T_1)e^{i\theta_2(T_1)},\\
&D_1A=\frac{1}{2}(\dot{a}+ia\dot{\theta}_1)e^{i\theta_1},\ D_1C=\frac{1}{2}(\dot{c}+ic\dot{\theta}_2)e^{i\theta_2},\\
&H(T_1)=\frac{1}{2}h(T_1)e^{i\theta_3(T_1)},\ Y(T_1)=\frac{1}{2}y(T_1)e^{i\theta_4(T_1)},\\
&D_1H=\frac{1}{2}(\dot{h}+ih\dot{\theta}_3)e^{i\theta_3},D_1Y=\frac{1}{2}(\dot{y}+iy\dot{\theta}_4)e^{i\theta_4},
\end{aligned}\right\} \tag{17}$$

where $\theta_1,\theta_2,\theta_3$, and θ_4 are the motion phases. The steady-state amplitudes of the system and controller motion are presented as a,c,h , and y , respectively.

The following amplitude-phase modulating equations are obtained by converting Eq (17) into Eq (16), while taking $\dot{\theta}_2=\dot{\varphi}_2-\dot{\varphi}_1+\sigma_1-\sigma_2$ and $\dot{\theta}_4=\dot{\varphi}_4-\dot{\varphi}_3+\sigma_3-\sigma_4$ into consideration:

$$\left.\begin{aligned}
&\dot{a}=-\mu_1a-\frac{\gamma_2\gamma_4}{2}\frac{1}{\delta_1^2+\omega_1^2}a+\frac{1}{2}\frac{\omega_2}{\omega_1}\gamma_1c\cos\varphi_2+\frac{f_1}{2\omega_1}\left(\sin\varphi_1-\cos\varphi_1\right),\\
&a\dot{\varphi}_1=a\sigma_1-\frac{3}{8\omega_1}\beta_2a^3+\frac{\gamma_2\gamma_4}{2\omega_1}\frac{\delta_1}{\delta_1^2+\omega_1^2}a-\frac{1}{2}\frac{\omega_2}{\omega_1}\gamma_1c\sin\varphi_2+\frac{f_1}{2\omega_1}\left(\cos\varphi_1+\sin\varphi_1\right),
\end{aligned}\right\} \tag{18}$$

$$\left.\begin{aligned}
&\dot{h}=-\mu_2h-\frac{\lambda_2\lambda_4}{2}\frac{1}{\delta_2^2+\omega_3^2}h+\frac{1}{2}\frac{\omega_4}{\omega_3}\lambda_1y\cos\varphi_4+\frac{f_2}{2\omega_3}\left(\sin\varphi_3-\cos\varphi_3\right),\\
&h\dot{\varphi}_3=h\sigma_3-\frac{3}{8\omega_3}\beta_4h^3+\frac{\lambda_2\lambda_4}{2\omega_3}\frac{\delta_2}{\delta_2^2+\omega_3^2}h-\frac{1}{2}\frac{\omega_4}{\omega_2}\lambda_1y\sin\varphi_4+\frac{f_2}{2\omega_3}\left(\cos\varphi_3+\sin\varphi_3\right),
\end{aligned}\right\} \tag{19}$$

$$\left.\begin{aligned}
&\dot{c}=-\frac{1}{2}\alpha_1c-\frac{1}{2}\frac{\omega_1}{\omega_2}\gamma_3a\cos\varphi_2,\\
&c\dot{\varphi}_2=\frac{1}{2}\frac{\omega_1}{\omega_2}\gamma_3a\sin\varphi_2-\frac{3}{8\omega_1}\beta_2a^2c+\frac{\gamma_2\gamma_4}{2\omega_1}\frac{\delta_1}{\delta_1^2+\omega_1^2}c-\frac{1}{2}\frac{\omega_2}{\omega_1}\gamma_1\frac{c^2}{a}\sin\varphi_2+\frac{cf_1}{2a\omega_1}\left(\cos\varphi_1+\sin\varphi_1\right)+c\sigma_2,
\end{aligned}\right\} \tag{20}$$

$$\left.\begin{aligned}
&\dot{y}=-\frac{1}{2}\alpha_2y-\frac{1}{2}\frac{\omega_3}{\omega_4}\lambda_3h\cos\varphi_4,\\
&y\dot{\varphi}_4=\frac{1}{2}\frac{\omega_3}{\omega_4}\lambda_3h\sin\varphi_4-\frac{3}{8\omega_3}\beta_4h^2y+\frac{\lambda_2\lambda_4}{2\omega_3}\frac{\delta_2}{\delta_2^2+\omega_3^2}y-\frac{1}{2}\frac{\omega_4}{\omega_2}\lambda_1\frac{y^2}{h}\sin\varphi_4+\frac{yf_2}{2h\omega_3}\left(\cos\varphi_3+\sin\varphi_3\right)+y\sigma_4,
\end{aligned}\right\} \tag{21}$$

where $\varphi_1=\sigma_1T_1-\theta_1,\varphi_2=\sigma_2T_1-\theta_1+\theta_2,\ \varphi_3=\sigma_3T_1-\theta_3,\varphi_4=\sigma_4T_1-\theta_3+\theta_4$. The stability of the equilibrium solutions of Eqs (18)–(21) as a function of parameters $\omega_1,\mu_1,\gamma_1,\gamma_2,\gamma_3,\gamma_4,\ f_1$, and c will be examined in order to assess the control law's performance.

5. Fixed-point solution

A fixed point in a steady-state solution to Eqs (18)–(21) could be found by stroking $\dot{a}=\dot{c}=0,\dot{\varphi}_1=\dot{\varphi}_2=0,\ \dot{h}=\dot{y}=0,\dot{\varphi}_3=\dot{\varphi}_4=0$.

$$\left.\begin{aligned}\frac{f_1}{2\omega_1}\left(\cos\varphi_1+\sin\varphi_1\right)&=-a\sigma_1+\frac{3}{8\omega_1}\beta_2a^3-\frac{\gamma_2\gamma_4}{2\omega_1}\frac{\delta_1}{\delta_1^2+\omega_1^2}a+\frac{1}{2}\frac{\omega_2}{\omega_1}\gamma_1c\sin\varphi_2\\ \frac{f_1}{2\omega_1}\left(\sin\varphi_1-\cos\varphi_1\right)&=\mu_1a+\frac{\gamma_2\gamma_4}{2}\frac{1}{\delta_1^2+\omega_1^2}a-\frac{1}{2}\frac{\omega_2}{\omega_1}\gamma_1c\cos\varphi_2\end{aligned}\right\},\tag{22}$$

$$\left.\begin{aligned}\frac{f_2}{2\omega_3}\left(\cos\varphi_3+\sin\varphi_3\right)&=-a\sigma_3+\frac{3}{8\omega_3}\beta_4h^3-\frac{\lambda_2\lambda_4}{2\omega_3}\frac{\delta_2}{\delta_2^2+\omega_3^2}a+\frac{1}{2}\frac{\omega_4}{\omega_3}\lambda_1y\sin\varphi_4\\ \frac{f_2}{2\omega_3}\left(\sin\varphi_3-\cos\varphi_3\right)&=\mu_2h+\frac{\lambda_2\lambda_4}{2}\frac{1}{\delta_2^2+\omega_3^2}h-\frac{1}{2}\frac{\omega_4}{\omega_3}\lambda_1y\cos\varphi_4\end{aligned}\right\},\tag{23}$$

$$\left.\begin{aligned}\sin\varphi_2&=\frac{2\omega_2c\left(\sigma_1-\sigma_2\right)}{\gamma_3\omega_1a}\\ \cos\varphi_2&=\frac{-\alpha_1\omega_2c}{\gamma_3\omega_1a}\end{aligned}\right\},\tag{24}$$

$$\left.\begin{aligned}\sin\varphi_4&=\frac{2\omega_4h\left(\sigma_3-\sigma_4\right)}{\lambda_3\omega_3h}\\ \cos\varphi_4&=\frac{-\alpha_2\omega_4y}{\lambda_3\omega_3h}\end{aligned}\right\}.\tag{25}$$

Squaring and subsequently adding Eqs (24) and (25) yields

$$\left.\begin{aligned}\left(\frac{\gamma_3\omega_1a}{2\omega_2}\right)^2&=\left(c\left(\sigma_1-\sigma_2\right)\right)^2+\left(\frac{1}{2}\alpha_1c\right)^2\\ \left(\frac{\lambda_3\omega_3h}{2\omega_4}\right)^2&=\left(y\left(\sigma_3-\sigma_4\right)\right)^2+\left(\frac{1}{2}\alpha_2y\right)^2\end{aligned}\right\}.\tag{26}$$

By inserting Eq (24) into (22), and (25) into (23), we obtain

$$\left.\begin{aligned}\frac{f_1}{2\omega_1}\left(\cos\varphi_1+\sin\varphi_1\right)&=-a\sigma_1+\frac{3}{8\omega_1}\beta_2a^3-\frac{\gamma_2\gamma_4}{2\omega_1}\frac{\delta_1}{\delta_1^2+\omega_1^2}a+\left(\frac{\omega_2}{\omega_1}\right)^2\left(\frac{\gamma_1c^2}{\gamma_3a}\right)\left(\sigma_1-\sigma_2\right)\\ \frac{f_1}{2\omega_1}\left(\sin\varphi_1-\cos\varphi_1\right)&=\mu_1a+\frac{\gamma_2\gamma_4}{2}\frac{1}{\delta_1^2+\omega_1^2}a+\frac{1}{2}\left(\frac{\omega_2}{\omega_1}\right)^2\left(\frac{\alpha_1\gamma_1c^2}{\gamma_3a}\right)\end{aligned}\right\},\tag{27}$$

$$\left.\begin{aligned}\frac{f_2}{2\omega_3}\left(\cos\varphi_3+\sin\varphi_3\right)&=-h\sigma_3+\frac{3}{8\omega_3}\beta_4h^3-\frac{\lambda_2\lambda_4}{2\omega_3}\frac{\delta_2}{\delta_2^2+\omega_3^2}h+\left(\frac{\omega_4}{\omega_3}\right)^2\left(\frac{\lambda_1y^2}{\lambda_3h}\right)\left(\sigma_3-\sigma_4\right)\\ \frac{f_2}{2\omega_3}\left(\sin\varphi_3-\cos\varphi_3\right)&=\mu_2h+\frac{\lambda_2\lambda_4}{2}\frac{1}{\delta_2^2+\omega_3^2}h+\frac{1}{2}\left(\frac{\omega_4}{\omega_2}\right)^2\left(\frac{\alpha_2\lambda_1y^2}{\lambda_3h}\right)\end{aligned}\right\}.\tag{28}$$

Squaring and subsequently adding Eq (27), as well as Eqs (28a) and (28b), yields:

$$\left.\begin{aligned}\left(\frac{f_1}{\sqrt{2}\omega_1}\right)^2&=\left(-a\sigma_1+\frac{3}{8\omega_1}\beta_2a^3-\frac{\gamma_2\gamma_4}{2\omega_1}\frac{\delta_1}{\delta_1^2+\omega_1^2}a+\left(\frac{\omega_2}{\omega_1}\right)^2\left(\frac{\gamma_1c^2}{\gamma_3a}\right)(\sigma_1-\sigma_2)\right)^2+\left(\mu_1a+\frac{\gamma_2\gamma_4}{2}\frac{1}{\delta_1^2+\omega_1^2}a+\frac{1}{2}\left(\frac{\omega_2}{\omega_1}\right)^2\left(\frac{\alpha_1\gamma_1c^2}{\gamma_3a}\right)\right)^2\\\left(\frac{f_2}{\sqrt{2}\omega_3}\right)^2&=\left(-h\sigma_3+\frac{3}{8\omega_3}\beta_4h^3-\frac{\lambda_2\lambda_4}{2\omega_3}\frac{\delta_2}{\delta_2^2+\omega_3^2}h+\left(\frac{\omega_4}{\omega_3}\right)^2\left(\frac{\lambda_1y^2}{\lambda_3h}\right)(\sigma_3-\sigma_4)\right)^2+\left(\mu_2h+\frac{\lambda_2\lambda_4}{2}\frac{1}{\delta_2^2+\omega_3^2}h+\frac{1}{2}\left(\frac{\omega_4}{\omega_2}\right)^2\left(\frac{\alpha_2\lambda_1y^2}{\lambda_3h}\right)\right)^2\end{aligned}\right\}. \quad (29)$$

The frequency response given by Eqs (26) and (28) corresponds to the practical case describing the behavior of the system's steady-state solutions, i.e., $(a\neq 0, c\neq 0, h\neq 0 \, and \, y\neq 0)$.

6. Nonlinear solution stability

The eigenvalues of the Jacobian matrix on the right-hand side of Eqs (18)–(21) are employed to assess the stability of the equilibrium solution. If the real part of each eigenvalue is negative, the corresponding equilibrium solution is asymptotically stable. Conversely, if the real part of any eigenvalue is positive, the corresponding equilibrium solution becomes unstable. To establish the stability requirements, it is necessary to analyze the behavior of small perturbations from the steady-state solutions $(a_{10}, c_{10}, h_{10}, y_{10}, \varphi_{10}, \varphi_{20}, \varphi_{30} \, and \, \varphi_{40})$. Thus, we assume that

$$\left.\begin{aligned}a_1=a_{10}+a_{11}, c_1=c_{10}+c_{11}, h_1=h_{10}+h_{11}, y_1=y_{10}+y_{11}, \varphi_1=\varphi_{10}+\varphi_{11},\\ \varphi_2=\varphi_{20}+\varphi_{21}, \varphi_3=\varphi_{30}+\varphi_{31} \, and \, \varphi_4=\varphi_{40}+\varphi_{41}\end{aligned}\right). \quad (30)$$

Let $(a_{10}, c_{10}, h_{10}, y_{10}, \varphi_{10}, \varphi_{20}, \varphi_{30} \, and \, \varphi_{40})$ denote quantities satisfying Eqs (22)–(25), while $(a_{11}, c_{11}, h_{11}, y_{11}, \varphi_{11}, \varphi_{21}, \varphi_{31} \, and \, \varphi_{41})$ represents perturbations that are considered small in comparison to $(a_{10}, c_{10}, h_{10}, y_{10}, \varphi_{10}, \varphi_{20}, \varphi_{30} \, and \, \varphi_{40})$. By substituting Eq (30) into Eqs (18)–(21) and retaining only the terms linear in $(a_{11}, c_{11}, h_{11}, y_{11}, \varphi_{11}, \varphi_{21}, \varphi_{31} \, and \, \varphi_{41})$, the following expressions are obtained:

$$\left.\begin{aligned}\dot{a}_{11}&=r_{11}a_{11}+r_{12}\varphi_{11}+r_{13}c_{11}+r_{14}\varphi_{21}\\\dot{\varphi}_{11}&=r_{21}a_{11}+r_{22}\varphi_{11}+r_{23}c_{11}+r_{24}\varphi_{21}\\\dot{c}_{11}&=r_{31}a_{11}+r_{32}\varphi_{11}+r_{33}c_{11}+r_{34}\varphi_{21}\\\dot{\varphi}_{21}&=r_{41}a_{11}+r_{42}\varphi_{11}+r_{43}c_{11}+r_{44}\varphi_{21}\end{aligned}\right\}, \quad (31)$$

$$\left.\begin{aligned}\dot{h}_{11}&=r_{55}h_{11}+r_{56}\varphi_{31}+r_{57}y_{11}+r_{58}\varphi_{41}\\\dot{\varphi}_{31}&=r_{65}h_{11}+r_{66}\varphi_{31}+r_{67}y_{11}+r_{68}\varphi_{41}\\\dot{y}_{11}&=r_{75}h_{11}+r_{76}\varphi_{31}+r_{77}y_{11}+r_{78}\varphi_{41}\\\dot{\varphi}_{41}&=r_{85}h_{11}+r_{86}\varphi_{31}+r_{87}y_{11}+r_{88}\varphi_{41}\end{aligned}\right\}, \quad (32)$$

where $(r_{11}-r_{88})$ are given in the Appendix B. Equations (31) and (32) can be displayed in the following matrix form:

$$\begin{bmatrix} \dot{a}_{11} \\ \dot{\varphi}_{11} \\ \dot{c}_{11} \\ \dot{\varphi}_{21} \\ \dot{h}_{11} \\ \dot{\varphi}_{31} \\ \dot{y}_{11} \\ \dot{\varphi}_{41} \end{bmatrix} = [J] \begin{bmatrix} a_{11} \\ \varphi_{11} \\ c_{11} \\ \varphi_{21} \\ h_{11} \\ \varphi_{31} \\ y_{11} \\ \varphi_{41} \end{bmatrix}, \tag{33}$$

where J denotes the Jacobian matrix corresponding to Eqs (31) and (32). The eigenvalues of J can be expressed as

$$\lambda^8 + R_1\lambda^7 + R_2\lambda^6 + R_3\lambda^5 + R_4\lambda^4 + R_5\lambda^3 + R_6\lambda^2 + R_7\lambda^1 + R_8 = 0. \tag{34}$$

For the solution to remain stable, a necessary and sufficient requirement is that all eigenvalues possess negative real parts; otherwise, instability occurs. Based on the Routh-Hurwitz criterion, this requirement is fulfilled if and only if the determinant (D) and all of its principal minors are strictly positive, ensuring that all roots of Eq (34) lie in the left half of the complex plane.

$$D = \begin{bmatrix} \Gamma_1 & 1 & 0 & 0 & 0 & 0 & 0 & 0 \\ \Gamma_3 & \Gamma_2 & \Gamma_1 & 1 & 0 & 0 & 0 & 0 \\ \Gamma_5 & \Gamma_4 & \Gamma_3 & \Gamma_2 & \Gamma_1 & 1 & 0 & 0 \\ \Gamma_7 & \Gamma_6 & \Gamma_5 & \Gamma_4 & \Gamma_3 & \Gamma_2 & \Gamma_1 & 1 \\ 0 & \Gamma_8 & \Gamma_7 & \Gamma_6 & \Gamma_5 & \Gamma_4 & \Gamma_3 & \Gamma_2 \\ 0 & 0 & 0 & \Gamma_8 & \Gamma_7 & \Gamma_6 & \Gamma_5 & \Gamma_4 \\ 0 & 0 & 0 & 0 & 0 & \Gamma_8 & \Gamma_7 & \Gamma_6 \\ 0 & 0 & 0 & 0 & 0 & 0 & 0 & \Gamma_8 \end{bmatrix}. \tag{35}$$

7. Results and discussions

To analyze the numerical behavior of the system described by Eqs (1)–(6), the fourth-order Runge-Kutta algorithm was employed. The stability of the vertical conveyor system was further explored using the multiple scales method and the frequency response function, while the influence of various parameters on the behavior of the controlled system was evaluated. Finally, a comparison was carried out between the analytical predictions and the corresponding numerical results.

7.1. System behavior before control

The system's numerical behavior under the most critical resonance conditions was examined using the following parameters:

$$\omega_1=1.8, \mu_1=0.01, \beta_1=0.02, \beta_2=0.2, f_1=0.04, \Omega_1=1.8, \gamma_1=1, \gamma_2=1, \omega_2=1.8, \alpha_1=0.001, \gamma_3=1, \delta_1=0.4, \gamma_4=1.$$

Time histories of the two coupled modes are presented for the uncontrolled system under simultaneous resonance $\Omega_1 = \omega_1, \Omega_2 = \omega_2, \omega_1 = \omega_3, \omega_2 = \omega_4$ in Figure 2. In this case, the responses of both conveyor modes exhibit amplitudes of approximately 2.5, while the diagrams reveal the presence of multiple limit cycles.

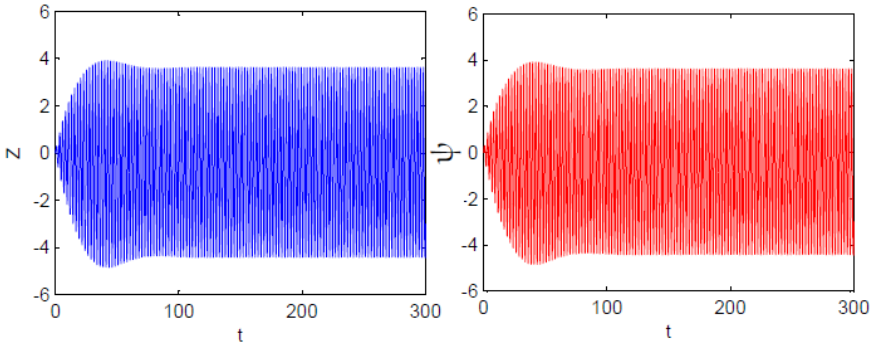

Figure 2. The amplitude of conveyor system without NINDF controller at $\Omega_1 = \omega_1 = 1.8, f_1 = 0.04$, and $\sigma_1 = 0$.

7.2. System behavior after control

Figure 3 illustrates the time histories of the two modes of the vertical conveyor system after implementing the NINDF controller. The steady-state amplitudes were reduced from approximately 3.6 to about 0.00002 for the two modes. This corresponds to a vibration reduction of about 99.9% compared to the uncontrolled case. The controller efficiencies, $(Ea = \text{amplitude with out controller/amplitude with controller})$ were approximately 239900 for the mode. It is also observed that the controller demonstrated high efficiency, requiring only a short time to stabilize the system under an external force of $f_1 = 0.04$. The control forces are depicted in Figure 4, where $f_1 = 0.4$ is ten times greater than the force applied in Figure 3. It is also noted that, at the start of the simulation, the system exhibited a temporary rise in amplitudes. Despite this increase, the system stabilized in approximately the same amount of time, which further demonstrates the effectiveness of the control strategy.

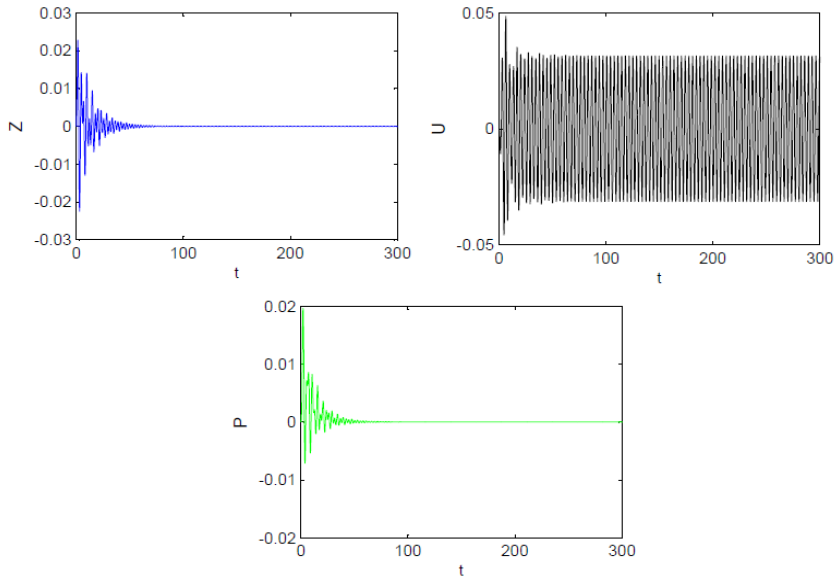

Figure 3. Responses for the main system and the (NINDF) controller $f_1 = 0.04$.

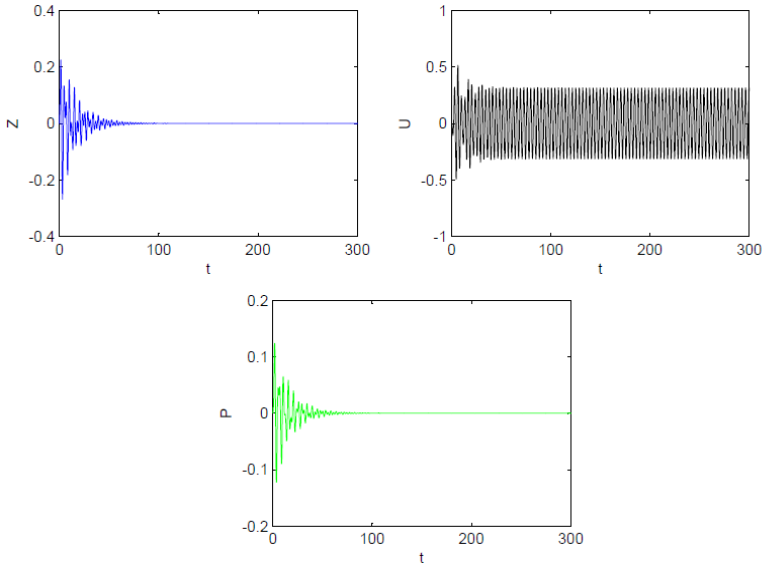

Figure 4. System responses with NINDF control $f_1 = 0.4$.

7.3. Curves of frequency response for the controlled system

The curves in Figure 5(a) and (b) illustrate the relationship between the detuning parameter σ_1 and the system response, whereas Figure 5(a) represents the first mode oscillation amplitude of the vertical conveyor, and Figure 5(b) denotes the NINDF response component. In both cases, two main resonance peaks can be observed, located at negative and positive values of σ_1. The solid lines represent stable solutions, while the dashed lines indicate unstable solutions, highlighting regions where sudden amplitude jumps may occur. As σ_1 approaches from the left (region A–B), the response amplitude rises steadily until reaching its maximum at point B, and the solution is stable, after which it declines sharply (B–C). The system then moves toward a second resonance (C–D), where instability is more prominent, before returning to lower amplitudes beyond point E. Physically, these patterns reveal how energy transfer into the system is maximized near resonance and diminishes outside it. From an engineering standpoint, identifying and avoiding the unstable regions around the resonance peaks is essential to prevent excessive vibrations and ensure safe operation. Figure 6(a) and (b) illustrate the system's steady-state amplitude responses under three different forcing amplitudes: $f_1 = 0.05, f_1 = 0.04 \, and \, f_1 = 0.03$. In both figures, two dominant resonance peaks appear symmetrically around $\sigma_1 = 0$, with their magnitudes increasing as the forcing amplitude grows. For $f_1 = 0.05$, the resonance peaks are the highest, indicating stronger energy transfer into the system. Reducing $f_1 = 0.04, f_1 = 0.03$ results in a noticeable suppression of the peak heights, reflecting lower vibrational energy levels. In Figure 6(a), the primary mode amplitude a exhibits a more pronounced sensitivity to changes in f_1, particularly near the left-hand resonance, while in Figure 6(b), the secondary mode amplitude h remains comparatively small in magnitude but follows a similar peak pattern. This behavior highlights the nonlinear resonance characteristics of the system, where even small changes in excitation amplitude can significantly influence the response. This also shows that both modes share similar resonance positions but differ in amplitude scale and sensitivity.

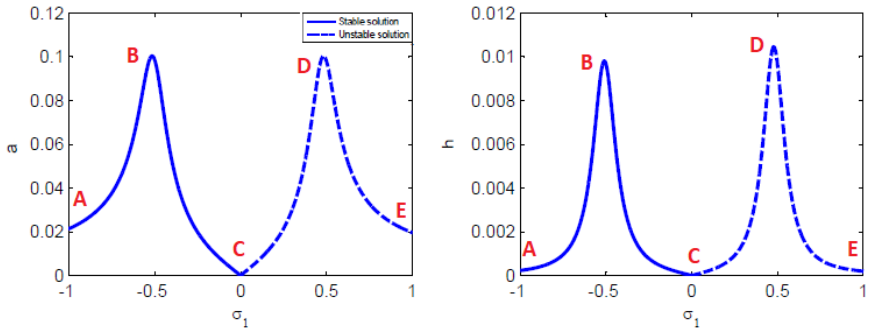

Figure 5. (a) Resonance curves for the main system; (b) NINDF controller.

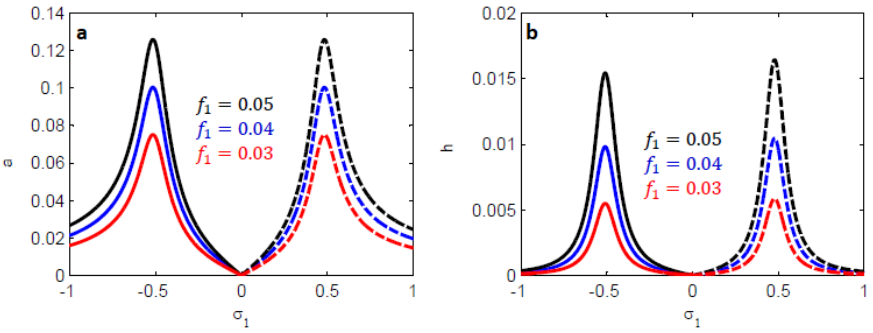

Figure 6. Effect of different values of the force f_1 on the frequency-response curves of (a) the main system and (b) the NINDF controller.

Figure 7(1)–(4) shows the effect of changing the parameters of the controlled system on the frequency response curves at different control values. Figures 7–10 illustrate the variations of amplitudes a and h as functions of used parameters. In Figure 7, the amplitude a exhibits a sharp peak, indicating a critical region of high sensitivity, with values of velocity signal coefficient (γ_1) increasing from 0.8 to 1.2. Similarly, Figure 8 shows the response of amplitudes a and h, where a distinct resonance peak becomes increasingly sharp, reflecting growing instability near resonance. Figure 9 highlights the influence of on amplitude a, where the observed peaks correspond to resonance conditions, and the spacing between curves demonstrates the strong effect of parameter changes on stability. Finally, Figure 10 presents amplitude h under varying, where the pronounced peak and curve spacing further emphasize the system's sensitivity and the direct impact of parameter variations on its overall dynamic behavior. Figure 11 shows the amplitudes a and h as functions of σ_1 for varying μ_1. The distinct peaks at $\sigma_1 = 0$ indicate critical response points. As μ_1 increases from 0.001 to 0.05, the peak magnitudes decrease, reflecting a more stable system with reduced sensitivity to changes in σ_1. This trend underscores the significance of μ_1 in influencing system dynamics and stability. When the natural frequency is relatively low, the system achieves higher stability at $\sigma_1 = 0$, meaning $\omega_1 = \omega_2$. Under these conditions, the maximum amplitudes for both the cantilever and the NINDF controller become larger, while the vibration range also expands. This behavior confirms that the NINDF controller performs with high efficiency in low-frequency scenarios, as presented in Figure 12.

Figure 13, with increased δ_1 from 1 to 1.3, clearly shows the strong effect of the control, as the peak amplitudes for both the cantilever response (a) and the controller response h are significantly reduced. The peaks also become narrower, indicating better frequency targeting and improved

system stability. This confirms that higher δ_1 values make the control more powerful in suppressing vibrations at resonance.

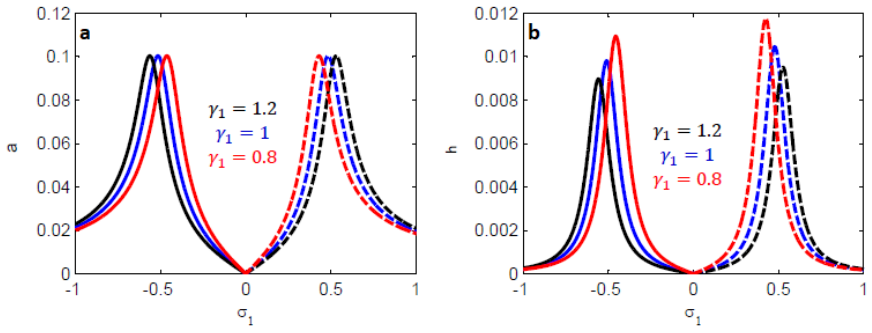

Figure 7. Effect of the controller velocity signal coefficient (γ_1) on system performance.

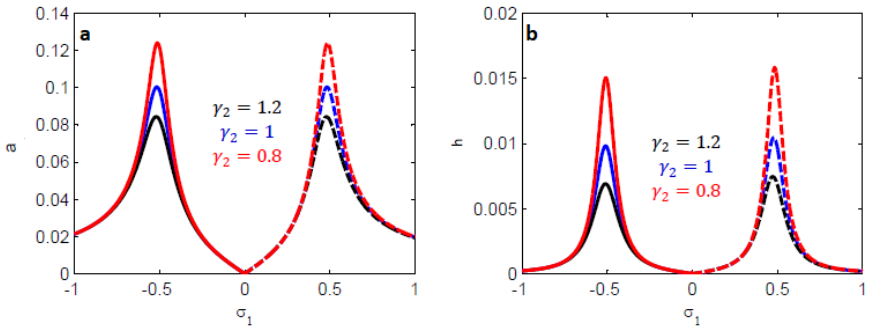

Figure 8. Effect of the controller displacement signal coefficient (γ_2) on system performance.

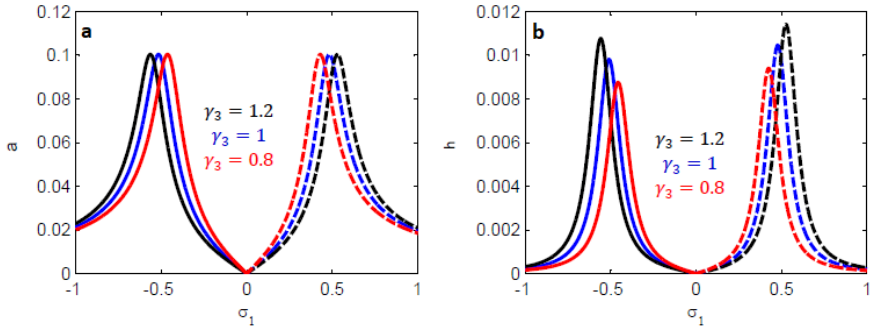

Figure 9. Effect of the controller velocity feedback coefficient (γ_3) on system performance.

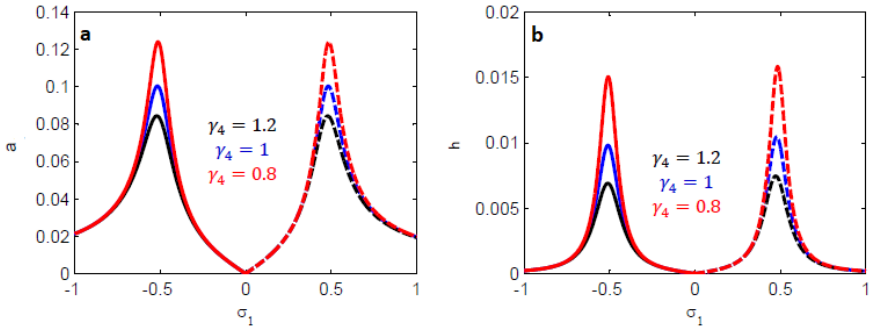

Figure 10. Effect of the controller displacement feedback coefficient (γ_4) on system performance.

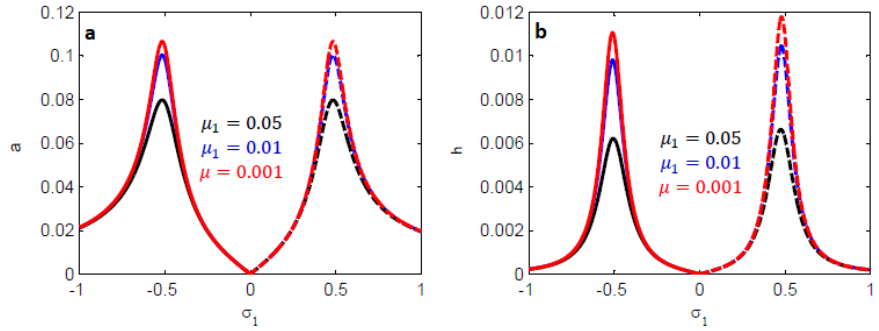

Figure 11. Effect of the damping coefficient μ_1 on frequency response curves of (a) the mean system and (b) the NINDF controller.

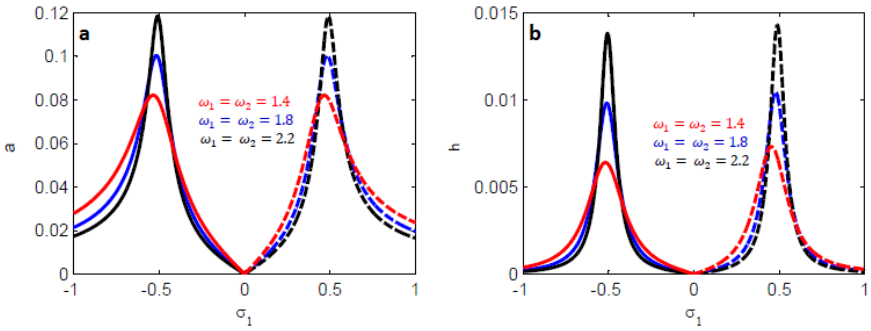

Figure 12. Effect of the nature frequency on frequency response curves of (a) the mean system and (b) the NINDF controller.

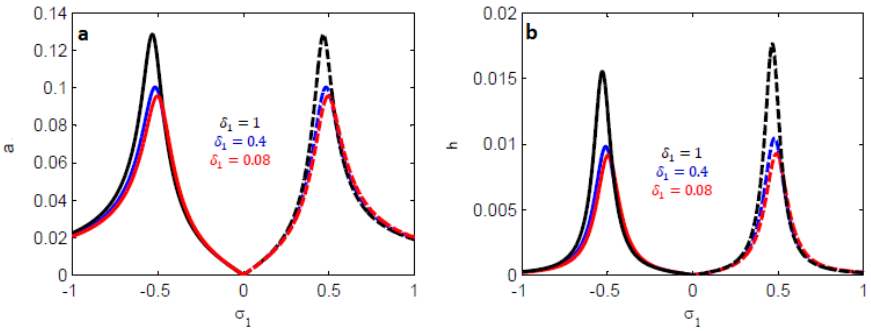

Figure 13. Effect of the lossy integrator's frequency δ_1 on frequency response curves of (a) the mean system and (b) the NINDF controller.

8. Comparison with previously published works

This study derives the governing equations for a vertical conveyor system, analyzing primary, subharmonic, and super-harmonic resonance. It explores vibration amplitudes, stability, and chaotic behavior in nonlinear systems [3]. As shown in Figure 14, when comparing the system's response under the four control strategies—PD, NSC, PPF, and NINDF—the differences in performance became quite clear [13]. With PD control, the oscillations stayed almost constant throughout the entire period, which means the system never really reached stability. Using NSC control, the oscillations started to fade gradually until the system finally settled at around t $\approx$ 1600 s. While this was an improvement over PD, the settling time was still very long [5]. On the other hand, PPF control showed faster damping, with the system stabilizing at about t $\approx$ 700 s [7]. The best results,

however, came from NINDF control, where the oscillations dropped very quickly and stability was achieved in just about t $\approx$ 80 s. This makes NINDF not only the fastest in reaching stability but also the most effective in improving the system's overall performance. Finally, the NINDF control, created by combining IRC and NDF, delivers remarkable results. It merges the resonance-handling of IRC with the strong damping of NDF, allowing the system to reach stability. This makes it far more effective and faster than all other control strategies.

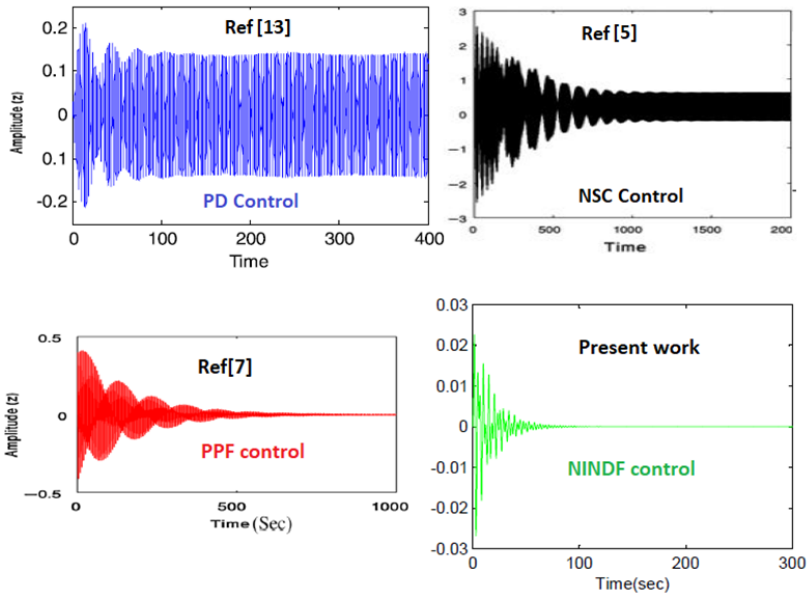

Figure 14. Comparison between different types of controllers.

9. Conclusions

This study investigates the vibrations of a vertical conveyor system subjected to an external excitation force and controlled using a nonlinear integral negative derivative feedback (NINDF) controller. A novel approach is proposed to mitigate the system's lateral vibrations by implementing the NINDF control strategy. The mathematical model is formulated by coupling two second-order nonlinear differential equations with first-order linear differential equations, representing both the conveyor system and the controller. To derive an approximate solution for the vibrating system, the method of multiple scales is employed. Frequency–response equations are then utilized to analyze the system's stability. Numerical simulations are carried out to evaluate the influence of all system parameters. Based on this analysis, the key findings are as follows:

- The vertical conveyor system's resonance cases are all examined, with a simultaneous primary and internal case, with $\Omega_1 = \omega_1, \Omega_2 = \omega_2, \omega_1 = \omega_3, \omega_2 = \omega_4$ being the worst.
- The NINDF control, created by combining IRC and NDF, delivers remarkable results. It merges the resonance-handling of IRC with the strong damping of NDF, allowing the system to reach stability.
- For the first mode (z), the amplitude is reduced to 99.9% compared to the amplitude of the uncontrolled system. This reduction indicates an effective response in mitigating oscillations, highlighting the system's improved stability and control performance, such that $E_a = 239900$.

- For the second mode (ψ), the amplitude is reduced to 98.7 compared to the amplitude of the uncontrolled system. This reduction indicates an effective response in mitigating oscillations, highlighting the system's improved stability and control performance, such that $E_a = 80$.
- The increase in the control coefficient $\gamma_i, i = 1,2,3,4$ sharpens the peaks, indicating greater system sensitivity and variations in stability.
- As the external excitation force $(f_1 \text{ and } f_2)$ increased, this impacted the controlled system's behavior.
- The response of the main system decreased with an increase in the damping coefficients μ_1, μ_2.
- Among the four control strategies, NINDF provides the fastest and most effective damping (~80 seconds), followed by PPF (~700 seconds), and then NSC (~1600 seconds), while PD is significantly unable to achieve stability.

Author contributions

Conceptualization: M. N. Abd El-Salam, Rageh K. Hussein, and R. E. Abdullah; Methodology: M. N. Abd El-Salam, and Mohamed Ibrahim Attia; Software: M. N. Abd El-Salam, and Asmaa M. Abd-Elal; Validation: Y. A. Amer, Rageh K. Hussein, and R. E. Abdullah; Formal analysis: O. M. Khaled, and R. E. Abdullah; Investigation: M. N. Abd El-Salam, and Rageh K. Hussein; Resources: M. N. Abd El-Salam, Rageh K. Hussein, and R. E. Abdullah; Data curation: R. E. Abdullah, and Asmaa M. Abd-Elal; Writing-original draft preparation: Rageh K. Hussein; Writing-review and editing: Y. A. Amer, and O. M. khaled; Visualization: Mohamed Ibrahim Attia; Project administration: M. N. Abd El-Salam, and Y. A. Amer; Funding acquisition: Rageh K. Hussein.

Use of Generative-AI tools declaration

The authors declare they have not used Artificial Intelligence (AI) tools in the creation of this article.

Acknowledgement

This work was supported and funded by the Deanship of Scientific Research at Imam Mohammad Ibn Saud Islamic University (IMSIU) (grant number IMSIU-DDRSP2503).

Conflict of interest

The authors declare that they have no known competing financial interests or personal relationships that could have appeared to influence the work reported in this paper.

Reference

1. B. Hüseyin, Computational dynamic analysis of unbalanced mass of vertical conveyer-elevator, *AIP Conf. Proc.*, **899** (2007), 712. https://doi.org/10.1063/1.2733453
2. H. Bayıroğlu, Nonlinear analysis of unbalanced mass of vertical conveyer-elevator, *AIP Conf. Proc.*, **1400** (2011), 66–70. https://doi.org/10.1063/1.3663087

3. H. Bayıroğlu, Nonlinear analysis of unbalanced mass of vertical conveyor: primary, subharmonic, and superharmonic response, *Nonlinear Dyn.*, **71** (2013), 93–107. https://doi.org/10.1007/s11071-012-0643-4
4. T. Kim, T. Rook, R. Singh, Super-and sub-harmonic response calculations for a torsional system with clearance nonlinearity using the harmonic balance method, *J. Sound Vib.*, **281** (2005), 965–993. https://doi.org/10.1016/j.jsv.2004.02.039
5. Y. Amer, A. El-Sayed, M. El-Salam, Non-linear saturation controller to reduce the vibrations of vertical conveyor subjected to external excitation, *ARJOM*, **11** (2018), 1–26. https://doi.org/10.9734/ARJOM/2018/44590
6. H. Bauomy, A. El-Sayed, Vibration performance of a vertical conveyor system under two simultaneous resonances, *Arch. Appl. Mech.*, **88** (2018), 1349–1368. https://doi.org/10.1007/s00419-018-1375-9
7. A. El-Sayed, H. Bauomy, Nonlinear analysis of vertical conveyor with positive position feedback (PPF) controllers, *Nonlinear Dyn.*, **83** (2016), 919–939. https://doi.org/10.1007/s11071-015-2377-6
8. F. Zhang, Y. Li, Existence and uniqueness of periodic solutions for a kind of duffing type p-Laplacian equation, *Nonlinear Anal.-Real*, **9** (2008), 985–989. https://doi.org/10.1016/j.nonrwa.2007.01.013
9. H. Gao, B. Liu, Existence and uniqueness of periodic solutions for forced Rayleigh-type equations, *Appl. Math. Comput.*, **211** (2009), 148–154. https://doi.org/10.1016/j.amc.2009.01.051
10. L. Cveticanin, Analytic approach for the solution of the complex-valued strong non-linear differential equation of Duffing type, *Physica A*, **297** (2001), 348–360. https://doi.org/10.1016/S0378-4371(01)00228-X
11. M. Rashidi, E. Erfani, New analytical method for solving Burgers' and nonlinear heat transfer equations and comparison with HAM, *Comput. Phys. Commun.*, **180** (2009), 1539–1544. https://doi.org/10.1016/j.cpc.2009.04.009
12. S. Mohimanianpour, M. Rashidi, Comparison of DTM and HAM solutions of energy equation of steady and fully developed flow in a circular tube, *Contemporary Mathematics and Statistics*, **1** (2013), 109–122. https://doi.org/10.7726/cms.2013.1008
13. Y. Hamed, H. Alotaibi, E. El-Zahar, Nonlinear vibrations analysis and dynamic responses of a vertical conveyor system controlled by a proportional derivative controller, *IEEE Access*, **8** (2020), 119082–119093. https://doi.org/10.1109/ACCESS.2020.3005377
14. Y. Amer, R. Abdullah, O. Khaled, A. Mahdy, M. El-Salam, Vibration control of smooth and discontinuous oscillator via negative derivative feedback, *J. Vib. Eng. Technol.*, **12** (2024), 2351–2363. https://doi.org/10.1007/s42417-024-01539-1
15. M. Namavar, A. Fleming, M. Aleyaasin, K. Nakkeeran, S. Aphale, An analytical approach to integral resonant control of second-order systems, *IEEE-ASME Trans. Mech.*, **19** (2013), 651–659. https://doi.org/10.1109/TMECH.2013.2253115
16. C. He, D. Tian, G. Moatimid, H. Salman, M. Zekry, Hybrid Rayleigh-Van der Pol-Duffing oscillator: stability analysis and controller, *J. Low Freq. Noise Vib. A.*, **41** (2021), 244–268. https://doi.org/10.1177/146134842110264

17. Y. Amer, A. El-Sayed, M. Abd El-Salam, Position and velocity time delay for suppression vibrations of a hybrid Rayleigh-Van der Pol-Duffing oscillator, *Sound Vib.*, **54** (2020), 149. https://doi.org/10.32604/sv.2020.08469
18. A. Shref, Y. Amer, M. Abd El-Salam, O. Khaled, E. Youssef, Vibration control of nonlinear dynamical system via negative cubic velocity feedback, *ERU Research Journal*, **4** (2025), 2630–2643. https://doi.org/10.21608/erurj.2025.331356.1197
19. Y. Amer, R. Hussein, S. Abu Alrub, A. Elgazzar, T. Salman, F. Mousa, et al., Suppressing nonlinear resonant vibrations via NINDF control in beam structures, *Mathematics*, **13** (2025), 2137. https://doi.org/10.3390/math13132137
20. H. Bauomy, Y. Amer, A. Elsayed, M. Agwa, A vibration analysis of the permanent magnet synchronous motor under the effect of proportional derivative control, *Phys. Scr.*, **99** (2024), 055233. https://doi.org/10.1088/1402-4896/ad398b
21. A. Amer, M. Abd EL-Salam, Negative derivative feedback controller for repressing vibrations of the hybrid Rayleigh-Van der Pol-Duffing oscillator, *Nonlinear Phenom. Com.*, **25** (2022), 217–228. https://doi.org/10.33581/1561-4085-2022-25-3-217-228
22. L. Ge, J. Song, Y. Shen, C. Liu, Q. Fu, S. Song, et al., Model predictive torque control of a novel multilevel power converter for four-phase SRMs, *IEEE Trans. Ind. Electron.*, in press. https://doi.org/10.1109/TIE.2025.3594416
23. X. Fang, Y. Hu, C. Zhu, S. An, L. Chen, Size-dependent vibration of laminated functionally graded curved beams covered with piezoelectric layers, *Mech. Adv. Mater. Struc.*, **30** (2023), 3257–3266. https://doi.org/10.1080/15376494.2022.2072546
24. C. Liu, J. Xu, X. Yue, RBF neural network-based cooperative electromagnetic takeover control for large-scale failed spacecraft, *IEEE Trans. Aero. Elec. Syst.*, in press. https://doi.org/10.1109/TAES.2025.3624706
25. A. Nayfeh, *Introduction to perturbation techniques*, Hoboken: John Wiley & Sons, 2011.
26. J. Kevorkian, J. Cole, *Multiple scale and singular perturbation methods*, New York: Springer Science & Business Media, 2012. https://doi.org/10.1007/978-1-4612-3968-0

Appendix A

Coefficients mentioned in Eq (14) are determined as follows:

$$N_1=\left(\frac{\beta_1 A^2}{3\omega_1^2}\right), N_2=\left(-\frac{2\beta_1 A\bar{A}}{\omega_1^2}\right), N_3=\left(\frac{\beta_2 A^3}{8\omega_1^2}\right), N_4=\left(\frac{i\omega_2\gamma_1 c}{\omega_1^2-\omega_2^2}\right), N_5=\left(\frac{f_1}{2(\omega_1^2-\Omega_1^2)}\right), N_6=\left(\frac{-i\omega_2\gamma_3 A}{\omega_2^2-\omega_1^2}\right),$$

$$N_7=\gamma_4\left(\frac{\beta_1 A^2(\delta_1-2i\omega_1)}{3\omega_1^2(\delta_1^2+4\omega_1^2)}\right), N_9=\left(-\frac{2\beta_1 A\bar{A}}{\omega_1^2\delta_1}\right), N_8=\left(\frac{\beta_2 A^3(\delta_1-3i\omega_1)}{8\omega_1^2(\delta_1^2+9\omega_1^2)}\right),$$

$$N_{10}=\left(\frac{i\omega_2\gamma_1 C(\delta_1-i\omega_2)}{(\omega_1^2-\omega_2^2)(\delta_1^2+\omega_2^2)}\right), N_{11}=\left(\frac{f_1(\delta_1-i\Omega_1)}{2(\omega_1^2-\Omega_1^2)(\delta_1^2+\Omega_1^2)}\right),$$

$$N_{12}=\left(-\left(\frac{\delta_1-i\omega_1}{\delta_1^2+\omega_1^2}\right)^2\gamma_4 D_1 A\right), N_{13}=\left(-D_1 G T_0\right),$$

$$L_1=\left(\frac{\beta_3E^2}{3\omega_3^2}\right),L_2=\left(\frac{-2\beta_3E\bar{E}}{\omega_3^2}\right),L_3=\left(\frac{\beta_4E^3}{8\omega_3^2}\right),L_4=\left(\frac{i\omega_4\lambda_1Y}{\omega_3^2-\omega_4^2}\right),$$
$$L_5=\left(\frac{f_2}{2(\omega_3^2-\Omega_2^2)}\right),L_6=\nu_1=\left(\frac{-i\omega_4\lambda_3E}{\omega_4^2-\omega_3^2}\right),$$

$$L_7=\left(\lambda_4\left(\frac{\beta_3H^2(\delta_2-2i\omega_3)}{3\omega_3^2(\delta_2^2+4\omega_3^2)}\right)\right),L_9=\left(-\frac{2\beta_3H\bar{H}}{\omega_3^2\delta_2}\right),L_8=\left(\frac{\beta_4H^3(\delta_2-3i\omega_3)}{8\omega_3^2(\delta_2^2+9\omega_3^2)}\right),$$
$$L_{10}=\left(\frac{i\omega_4\lambda_1Y(\delta_2-i\omega_4)}{(\omega_3^2-\omega_4^2)(\delta_2^2+\omega_4^2)}\right),L_{11}=\left(\frac{f_2(\delta_2-i\Omega_2)}{2(\omega_3^2-\Omega_2^2)(\delta_2^2+\Omega_2^2)}\right),$$
$$L_{12}=\left(-\left(\frac{\delta_2-i\omega_3}{\delta_2^2+\omega_3^2}\right)^2\lambda_4D_1H\right),L_{13}=\left(-D_1MT_0\right),$$

Appendix B

Coefficients mentioned in Eqs (31) and (32) are determined as follows:

$$\mathrm{r}_{11}=\left(-\mu_1-\frac{(1/2)\gamma_2\gamma_4\omega_1}{\delta_1^2+\omega_1^2}\right),\mathrm{r}_{12}=\left(\frac{1}{2}\frac{f_1\left(\cos(\varphi_{10})+\sin(\varphi_{10})\right)}{\omega_1}\right),$$
$$\mathrm{r}_{13}=\left(\frac{1}{2}\frac{\omega_2\gamma_1\cos(\varphi_{20})}{\omega_1}\right),\mathrm{r}_{14}=\left(\frac{-1}{2}\frac{\omega_2\gamma_1\sin(\varphi_{20})}{\omega_1}\right),$$

$$\mathrm{r}_{21}=\left(\frac{\sigma_1}{a_{10}}-\frac{9}{8}\frac{\beta_2a_{10}}{\omega_1}+\frac{1}{2}\frac{\gamma_2\gamma_4\delta_1}{\omega_1a_{10}\left(\delta_1^2+\omega_1^2\right)^2}\right),\mathrm{r}_{22}=\left(\frac{1}{2}\frac{f_1\left(\cos(\varphi_{10})-\sin(\varphi_{10})\right)}{a_{10}\omega_1}\right)$$
$$\mathrm{r}_{23}=\left(\frac{-1}{2}\frac{\omega_2\gamma_1\sin(\varphi_{20})}{a_{10}\omega_1}\right),\mathrm{r}_{24}=\left(-\frac{1}{2}\frac{\omega_2\gamma_1\cos(\varphi_{20})}{a_{10}\omega_1}\right),$$

$$\mathrm{r}_{31}=\left(-\frac{1}{2}\frac{\omega_1\gamma_3\cos(\varphi_{20})}{\omega_2}\right),\mathrm{r}_{32}=0,\mathrm{r}_{33}=-0.5\alpha_1,\mathrm{r}_{34}=\left(\frac{1}{2}\frac{\omega_1\gamma_3a_{10}\sin(\varphi_{20})}{\omega_2}\right),$$

$$r_{41}=\left(-\frac{3}{4}\frac{\beta_2 a_{10}}{\omega_1}+\frac{1}{2}\frac{\omega_1\gamma_3\,sin(\varphi_{20})}{c_{10}\omega_2}\right), r_{22}=\left(\frac{1}{2}\frac{f_1\left(\cos(\varphi_{10})-sin(\varphi_{10})\right)}{a_{10}\omega_1}\right),$$

$$r_{23}=\left(\frac{\sigma_2}{c_{10}}-\frac{1}{2}\frac{\omega_2\gamma_1\,sin(\varphi_{20})}{a_{10}\omega_1}-\frac{3}{8}\frac{\beta_2 a_{10}^2}{c_{10}\omega_1}+\frac{1}{2}\frac{\gamma_2\gamma_4\delta_1}{\omega_1 c_{10}\left(\delta_1^2+\omega_1^2\right)^2}+\frac{1}{2}\frac{f_1\left(\cos(\varphi_{10})+sin(\varphi_{10})\right)}{c_{10}a_{10}\omega_1}\right),$$

$$r_{24}=\left(\frac{1}{2}\frac{\omega_1\gamma_3 a_{10}\cos(\varphi_{20})}{c_{10}\omega_2}-\frac{1}{2}\frac{\omega_2\gamma_1 c_{10}\cos(\varphi_{20})}{a_{10}\omega_2}\right),$$

$$r_{55}=\left(-\mu_2-\frac{(1/2)\lambda_2\lambda_4\omega_3}{\delta_2^2+\omega_3^2}\right), r_{56}=\left(\frac{1}{2}\frac{f_2\left(\cos(\varphi_{30})+sin(\varphi_{30})\right)}{\omega_3}\right),$$

$$r_{57}=\left(\frac{1}{2}\frac{\omega_4\lambda_1\cos(\varphi_{40})}{\omega_3}\right), r_{58}=\left(\frac{-1}{2}\frac{\omega_4\lambda_1\,sin(\varphi_{40})}{\omega_3}\right),$$

$$r_{65}=\left(\frac{\sigma_3}{h_{10}}-\frac{9}{8}\frac{\beta_4 h_{10}}{\omega_3}+\frac{1}{2}\frac{\lambda_2\lambda_4\delta_2}{\omega_3 h_{10}\left(\delta_2^2+\omega_3^2\right)^2}\right), r_{66}=\left(\frac{1}{2}\frac{f_2\left(\cos(\varphi_{30})-sin(\varphi_{30})\right)}{h_{10}\omega_3}\right),$$

$$r_{67}=\left(\frac{-1}{2}\frac{\omega_4\lambda_1\,sin(\varphi_{40})}{h_{10}\omega_3}\right), r_{68}=\left(-\frac{1}{2}\frac{\omega_4\lambda_1\cos(\varphi_{40})}{h_{10}\omega_3}\right),$$

$$r_{75}=\left(-\frac{1}{2}\frac{\omega_3\lambda_3\cos(\varphi_{40})}{\omega_4}\right), r_{76}=0, r_{77}=-0.5\alpha_2, r_{78}=\left(\frac{1}{2}\frac{\omega_3\lambda_3 h_{10}\,sin(\varphi_{40})}{\omega_4}\right),$$

$$r_{85}=\left(-\frac{3}{4}\frac{\beta_4 h_{10}}{\omega_3}+\frac{1}{2}\frac{\omega_3\lambda_3\,sin(\varphi_{40})}{y_{10}\omega_4}\right), r_{86}=\left(\frac{1}{2}\frac{f_2\left(\cos(\varphi_{30})-sin(\varphi_{30})\right)}{h_{10}\omega_3}\right),$$

$$r_{87}=\left(\frac{\sigma_4}{y_{10}}-\frac{1}{2}\frac{\omega_4\lambda_1\,sin(\varphi_{40})}{h_{10}\omega_3}-\frac{3}{8}\frac{\beta_4 h_{10}^2}{y_{10}\omega_3}+\frac{1}{2}\frac{\lambda_2\lambda_4\delta_2}{\omega_3 y_{10}\left(\delta_2^2+\omega_3^2\right)^2}+\frac{1}{2}\frac{f_2\left(\cos(\varphi_{30})+sin(\varphi_{30})\right)}{y_{10}h_{10}\omega_3}\right),$$

$$r_{88}=\left(\frac{1}{2}\frac{\omega_3\lambda_3 h_{10}\cos(\varphi_{40})}{y_{10}\omega_4}-\frac{1}{2}\frac{\omega_4\lambda_1 y_{10}\cos(\varphi_{40})}{h_{10}\omega_4}\right).$$